Polarons: Energetics and their structural and electronic effects in $ATiO_3$ perovskite systems

Dylan Windsor and Haixuan Xu*
University of Tennessee-Knoxville, Knoxville, Tennessee 37996, USA

(Received 30 January 2023; accepted 10 April 2023; published 10 May 2023)

Understanding the formation of a polaron near vacancies in oxides is of vital importance for controlling defect properties and related functionalities. We examine the energetics and local structure of polarons in the vicinity of oxygen vacancies using density functional theory with the Hubbard on-site Coulombic correction. We systematically consider several $ATiO_3$ perovskite systems: cubic $SrTiO_3$ (c-STO), cubic $BaTiO_3$ (c-BTO), cubic $PbTiO_3$ (c-PTO), tetragonal $BaTiO_3$ (t-BTO), and tetragonal $PbTiO_3$ (t-PTO). The polaron formation energies vary by several orders of magnitude across the systems, where PTO systems have large polaron formation energies (~ -1.688 eV), c-BTO is intermediate (-0.234 eV), and c-STO and t-BTO have considerably smaller formation energies (< -0.01 eV). The formation of a polaron is found to influence the charge density, atomic displacement, and electronic structure, with higher polaron energies corresponding to larger charge density changes and greater displacements of the ions surrounding the oxygen vacancy, especially the displacement of the first nearest neighbor A-site. Finally, a comparison of the projected band structures shows fictitious in-gap states present in the delocalized picture of the system moving to the conduction and valence bands in the polaron solution of the system, indicating an incompleteness of the description of a vacancy without considering charge localization as in the polaron picture. In this paper, we provide fundamental properties of polarons near vacancies, which can be used to control and tune defect, charge transport, magnetoelectric, and multiferroic properties of perovskite oxides.

DOI: 10.1103/PhysRevMaterials.7.055004

I. INTRODUCTION

The intricately entangled lattice, charge, orbital, and spin degrees of freedom, from which the rich variety of tunable and technologically critical properties in the perovskite oxides arise, are known to interact with defects present in these materials, the most ubiquitous of which is the oxygen vacancy [1–3]. Many of the functional properties possessed by perovskites, such as colossal magnetoresistance [1], photovoltaic interactions [4], and multiferroism [1–3], result from the highly confined and correlated d orbitals present within the oxygen octahedra [2]. Then using oxygen vacancies to exert a degree of control over properties highly sensitive to this confinement is implied since oxygen vacancies directly alter the d-orbital environment. For example, it is known in photovoltaic perovskites that oxygen vacancies cause partial hybridization of adjacent metal orbitals, providing trapping and recombination sites within the lattice [4]. A similar dependency has been observed in the origins of the emergent multiferroic behavior in $PbTiO_3$, wherein oxygen vacancies in the TiO_6 octahedra produce an unequal distribution of the magnetization density in the first nearest neighbor (1NN) Ti-sites to induce ferromagnetism in the ferroelectric phase [5,6]. Furthermore, vacancy formation energies have been shown to depend on both the polarization and TiO_6 octahedral rotation in ferroelectric $PbTiO_3/SrTiO_3$ (PTO/STO) [7]. This begs a fundamental question about the nature of the charge-lattice interaction near vacancies in these materials, which can be investigated using a quasiparticle defined as a polaron.

A polaron is defined as charge localization coupled with a distortion of the lattice [8–11]. These quasiparticles have been found to significantly affect the physics in a variety of phenomena, including charge transport [10,12], colossal magnetoresistance [13], and multiferroism [14]. Polarons have been studied extensively in many systems [9], such as TiO_2 and its allotropes [8,15–18], $SrTiO_3$ [19,20], other transition metal oxides [8,21–24], and metal halide perovskites [14]. Reticcioli *et al.* [15] report polaron formation near oxygen vacancies at reduced surfaces of rutile TiO_2, where the polarons play a significant role in the adsorption of CO on the surface. Furthermore, Zhang *et al.* [21] report the mechanisms of polaron hopping and vacancy migration influence on one another on the (111) surfaces of CeO_2, giving rise to entangled movements between surface polarons and vacancies that effectively control charge transfer on the surface. Given the importance of polarons and their interactions with oxygen vacancies in oxides, it is essential to develop a comprehensive fundamental understanding of how the lattice, charge, orbital, spin, and defect degrees of freedom influence polaron properties. Recent advancements in experimental techniques and computational capability have enabled depth and breadth of exploration into polaron properties.

There are several experimental techniques often used to investigate polaron behavior, including transport measurements, photoluminescence, and optical and electron spectroscopies. Early studies of polarons were limited to transport measurements, like resistivity and the Seebeck coefficient, to show

*xhx@utk.edu

the existence of polarons [4,23–25]. However, it is difficult with transport techniques alone to understand the electronic transitions of charge carriers, to image the polarons themselves, or to precisely identify phonon mode couplings. In photoluminescence, electronic transitions can be accurately measured, though the nature of the polaron can be difficult to interpret from the data since both hole and electron polarons provide similar signals [9]. Scanning tunneling electron microscopy/spectroscopy (STM/STS) provides the capability to image polarons directly, as demonstrated by Setvin *et al.* [16] on allotropes of TiO_2. The technique shows that polaron formation in TiO_2 allotropes results from charge carriers donated by surface oxygen vacancies. However, the tunneling current used to make measurements in STM/STS can alter the polaron configurations or induce additional hopping [15,26]. Phonon modes can be identified using angle-resolved photoemission spectroscopy, but data interpretation for small polarons is under debate [9,27]. Since these difficulties impede development of a comprehensive understanding when using experimental techniques alone, computational methods, such as density functional theory (DFT), are of vital importance to studies of polarons.

Standard DFT suffers from a well-known self-interaction error when accounting for highly correlated electrons, providing instead a completely delocalized picture of electrons [9], making polaron modeling impossible. However, there are several popular schemes to account for this limitation: the Hubbard on-site correction (DFT+U) [28], the self-interaction correction scheme [29,30], or with hybrid functionals [31]. Of these three, including the Hubbard on-site U correction is the most computationally affordable and still provides reasonable agreement with experimental observations [32]. For example, DFT+U studies of TiO_2 agreed with experiments, confirming small polaron formation in rutile and large polaron formation in anatase, by interpreting the large optical phonon coupling data from optical spectroscopy [9,15,16,26]. In this case, DFT+U allowed a direct observation of the polaron formation and migration in both rutile and anatase, showing the differences in polaron transport mechanisms [32] and polaron interactions with vacancies in both allotropes [16]. Furthermore, Xu *et al.* [33] used DFT+U to investigate the effects of epitaxial strain on the polaron formation and migration in $BaTiO_3$, demonstrating magnetically active polarons can form under electron doping conditions. DFT+U may be used with great effectiveness to inform, elucidate, and corroborate experimental endeavors, in addition to providing powerful insight into the mechanisms of polaron behaviors in materials.

Despite these advancements, an understanding of vacancy and polaron interactions in perovskite oxides remains incomplete. Given the wealth of physical properties in perovskites dependent on these interactions, it is essential to establish a theoretical framework of vacancy-polaron interactions in these material systems. In this paper, we investigate the polaron energetics near oxygen vacancies in several well-studied titanates, including cubic $SrTiO_3$ (c-STO), $BaTiO_3$ (c-BTO), and $PbTiO_3$ (c-PTO), and tetragonal $BaTiO_3$ (t-BTO) and $PbTiO_3$ (t-PTO), allowing for systematic cross-examination of A-site effects. The electronic and structural changes after polaron formation are analyzed and compared with the delocalized picture. Correspondingly, the charge density, atomistic displacements, and electronic structure of the resulting polarons are elucidated to characterize the fingerprints of the polaron solution and provide a full description of the charge localization.

II. METHODOLOGY

All calculations are herein performed using DFT with a planar-augmented basis set [34] as implemented in VASP [35,36]. The exchange-correlation term is accounted for within the generalized gradient approximation (GGA) of the Perdew-Burke-Ernzerhof (PBE) functional [37] revised for solids, PBEsol [38]. For each system, a 3×3×3 supercell is used, based on results from Zhang *et al.* [39] for which convergence testing shows $E_{\text{cut}} = 550$ eV with a Monkhorst-Pack k-point grid of 2×2×2 to provide an excellent balance of accuracy and computational efficiency. Valence electron configurations for each species are as follows: Ti $3p3d4s$, O $2s2p$, Sr $4s4p5s$, Ba $5s5p6s$, and Pb $5d6s6p$. Within DFT+U, the choice of the +U parameter is significant for all properties calculated, and since there is no general choice that reproduces all necessary properties of a given material, the +U parameter is often chosen for agreement on the properties of interest [8,9,11,32], that is, empirically. Therefore, a rotationally invariant Hubbard U correction in the formalism of Dudarev *et al.* [28], $U_{\text{eff}} = 4.46$ eV, is applied to the Ti-3d orbitals since this value is known to accurately reproduce vacancy formation properties in the c-STO and PTO/STO system [7,8,39,40].

The oxygen vacancy formation energy was calculated according to [41]

$$E_f\left[V_{\text{O}}^q\right] = E_{\text{tot}}\left[V_{\text{O}}^q\right] - E_{\text{tot}}[\text{bulk}] - \sum_i n_i\mu_i + q(E_{\text{Fermi}} + E_{\text{VBM}} + \Delta V), \quad (1)$$

where $E_f[V_{\text{O}}^q]$ is the formation energy of a vacancy of charge state q. The first two energy terms $E_{\text{tot}}[V_{\text{O}}^q]$ and $E_{\text{tot}}[\text{bulk}]$ are the total energy of the supercell containing the vacancy and the total energy of the bulk supercell, respectively. The chemical potential μ_i of atoms added ($n_i > 0$) or removed ($n_i < 0$) is accounted for with the $\sum_i n_i\mu_i$ term. In this paper, the chemical potential of oxygen μ_i is −4.338 eV [39], the oxygen chemical potential. Finally, E_{Fermi} is the Fermi energy, E_{VBM} is the valence band maximum (VBM), and ΔV [41] accounts for the misalignment of the Fermi levels in the defected and bulk supercells.

To investigate the polaron properties near a vacancy in each system, a general procedure [16] is used to obtain the polaron solution via

$$E_{\text{pol}} = E_{\text{loc}}^{\text{rel}} - E_{\text{del}}^{\text{unrel}}, \quad (2)$$

where E_{pol} is the polaron formation energy, $E_{\text{loc}}^{\text{rel}}$ is the total energy of the relaxed-localized solution, and $E_{\text{del}}^{\text{unrel}}$ is the total energy of the unrelaxed-delocalized solution. In this paper, the $E_{\text{loc}}^{\text{rel}}$ term is the total energy of a completely relaxed supercell with two holes introduced (two electrons removed), and the $E_{\text{del}}^{\text{unrel}}$ term describes a supercell with two holes added but with the same structure as the relaxed neutral vacancy system. This

TABLE I. The lattice constants, a, c/a ratio, and neutral oxygen vacancy formation energy $E_f[V_O^X]$ are shown below. Each of the 3×3×3 supercell systems were relaxed under the criteria above to the lattice parameters given, after which a neutral oxygen vacancy was added to the system and atomic positions subsequently relaxed. For each system, neutral oxygen vacancy formation energies were calculated according to Eq. (1).

System	Phase	a(Å)	c/a	$E_f[V_O^X]$ (eV)	a(Å)	c/a	$E_f[V_O^X]$ (eV)
c-STO	$Pm\bar{3}m$	3.936	1	6.481	3.939 [39] 3.9067(9) [43]	1	6.576 [39]
c-BTO	$Pm\bar{3}m$	4.010	1	6.475	4.025 [44] 4.0354 [45]	1	6.63 [46]
c-PTO	$Pm\bar{3}m$	3.959	1	5.597	3.96 [47] 3.9692(1) [48]	1	—
t-BTO	$P4mm$	3.972	1.037	6.299	3.9934 [44] 3.9905 [45]	1.048 [44] 1.008 [45]	6.35 [49] 6.30 [50]
t-PTO	$P4mm$	3.874	1.091	5.742	3.876 [51] 3.9040(1) [48]	1.071 [51] 1.065 [48]	5.45(5) [51] 5.44 [50]

method is general for DFT+U and has been used previously in the work of Deskins and Dupuis [32] and recognized in the review on polarons by Franchini *et al.* [9]. When relaxation was conducted, Hellmann-Feynman forces were converged to < 0.01 eV/Å, and the total energy was converged to within 10^{-8} eV.

In this paper, each system is treated in this manner so the electronic and structural effects of the A-site change on polaron properties could be investigated. Polaron formation energetics are calculated and compared using Eq. (2) for each system. VESTA [42] is used to visualize both charge density and structural changes induced by the polaron formed. The electronic structure of these polaron formations is probed using orbital-resolved density of states (DOS) and projected-band structure calculations. Postanalysis of the electronic structure data is performed by plotting with a homemade Python script, where the differences in band structures between the polaron and delocalized bands are carefully filtered and highlighted.

III. RESULTS AND DISCUSSION

A. Lattice constant and neutral vacancy formation

The lattice parameter, c/a ratio, and $E_f[V_O^X]$ of each system were compared with the available literature, showing agreement with previous computational and experimental studies [39,43–51]. For example, lattice parameters of the cubic systems calculated by Piskunov *et al.* [47] using both hybrid and GGA functionals show consistent agreement to within $< 1\%$ of our calculated lattice parameters, and the same agreement to within $< 1\%$ is found with experimental studies of c-STO [43], c-BTO [45], and c-PTO [48] (Table I). Our lattice parameters and c/a ratios for the tetragonal systems show good agreement to within 1 and 2%, respectively, with other computational studies utilizing various functionals [44,51]. Furthermore, experimental studies show agreement to within 1% of computed lattice parameters for the tetragonal phases and to within 3% of our computed c/a ratios [45,48].

The neutral vacancy formation energy calculated using Eq. (1) agrees with the literature to within ~ 0.2 eV, giving the closeness in energy values of c-STO and c-BTO found in the literature. Furthermore, the structure of the neutral vacancy 1NN Ti- and O-sites calculated herein agrees to within < 0.01 Å with work performed by Evarestov *et al.* [52] using the PBE0 hybrid functional with a linear combination of atomic orbitals (LCAO) basis. We report agreement on the neutral vacancy formation energy to within ~ 0.05 eV for t-BTO [49,50] and ~ 0.3 eV for t-PTO [50,51] with previous computational studies, noting the differences in t-PTO with previous studies are likely due to the difference in functionals and computational setup. These neutral vacancy structures are used for subsequent calculations of the polaron properties.

B. Polaron energetics

The polaron formation energies were calculated for each system and compared (Table II), showing significant variation with the A-site of several orders of magnitude across the systems studied. In c-PTO, the polaron formation energy −1.688 eV shows a relatively large decrease in the system energy compared with the delocalized description [Eq. (2)]. Compared with this, the polaron formation energy decreases by one order of magnitude in c-BTO to −0.234 eV and by two orders of magnitude in c-STO to −0.007 eV (Table II). Furthermore, in the tetragonal systems, the polaron formation energy of t-PTO is calculated to be −1.823 eV, and the polaron formation energy t-BTO is nearly three orders of magnitude lower at −0.002 eV. Therefore, the polaron formation energy decreases as the A-site is varied from Sr < Ba < Pb, demonstrating the critical influence of the A-site on the polaron stability.

TABLE II. The polaron formation energy is given for each system, followed by the greatest change in charge density $\Delta\rho$, calculated by taking the largest difference at a given position between the localized and delocalized charge distribution.

Property	c-STO	c-BTO	c-PTO	t-BTO	t-PTO
Polaron formation energy (eV)	−0.007	−0.234	−1.688	−0.002	−1.823
$\Delta\rho$(max) (e/Å^3)	0.031	0.114	0.388	0.007	0.655

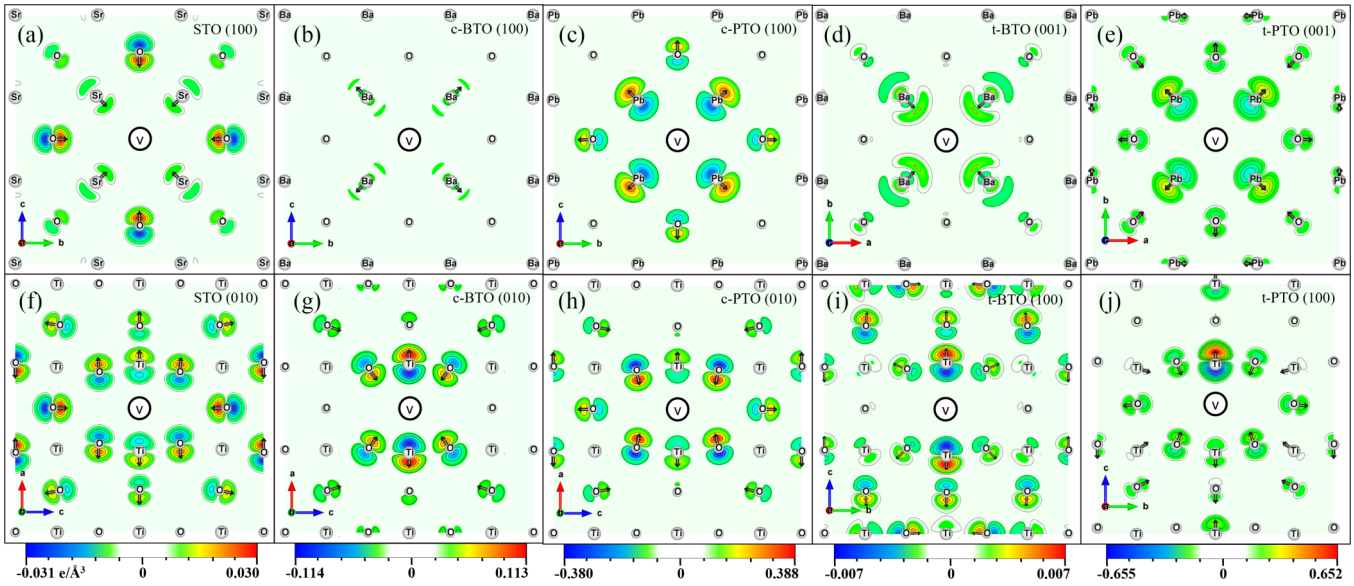

FIG. 1. The charge density differences between the relaxed polaron structure and delocalized structure, each with a separate color bar. Additionally, displacement directions for each atom with reference to the delocalized structure in each system are shown, scaled to highlight the features of the displacement directions for atoms. Each site is labeled with the species chemical symbol, and the vacancy is labeled with an encircled V.

The influence of the polaron on the charge density of the systems was assessed by taking the difference between the charge densities of the polaron solution [represented as $E_{\text{loc}}^{\text{rel}}$ in Eq. (2)] and the delocalized solution [represented as $E_{\text{del}}^{\text{unrel}}$ in Eq. (2)]. The largest difference at a given position between these charge densities $\mathbf{\Delta}\rho$ is shown in Table II for each system, where $\mathbf{\Delta}\rho$ is demonstrated to increase with decreasing polaron formation energy across the systems studied. We explore the A-site influence on the charge density more completely by visualizing the charge density differences in each of the systems below.

C. Charge density differences due to polarons

To understand the charge density changes and correlate them to the structures resulting from polaron formation, the charge density difference between the localized and delocalized solutions in Eq. (2) were generated for each system (Fig. 1). Please note the differences in magnitude of the color bar in each subfigure. The polaron responses of t-PTO and c-PTO are the strongest among the systems investigated, possessing charge density changes of 0.655 and 0.388 $\text{e}/\text{Å}^3$, respectively, while a mediate response of 0.114 $\text{e}/\text{Å}^3$ is found in c-BTO [Table II and Figs. 1(g), 1(h), and 1(j)], and a weak polaron response is observed in c-STO and t-BTO with responses of 0.031 and 0.007 $\text{e}/\text{Å}^3$, respectively [Table II and Figs. 1(f) and 1(i)]. Thus, the magnitudes of the charge density changes increase with decreasing polaron formation energy, as in Table II. This weak polaron picture in t-BTO agrees well with observations from work performed by Smyth [53], where it is stated that there is no evidence of trapped charge carriers in t-BTO based on transport measurements taken at varying temperatures and oxygen partial pressures. Furthermore, the band conduction nature of holes in t-BTO is corroborated by irreversible thermodynamic analysis conducted by Yoo [54] on the extensive range of oxygen partial pressure transport measurements of Yoo and Song [55], agreeing also with the weak polaron response observed in the current results for t-BTO.

On closer inspection, varying the A-site ion modifies the distribution and magnitude of the greatest charge density change. The charge density change is greatest on the 1NN A-site ions of the vacancy in c-PTO, the 1NN Ti-sites in c-BTO, and the second nearest neighbor (2NN) O-sites in c-STO. This shows the spatial influence of the A-site on the charge density distribution: The change density distribution of c-PTO is less spatially diffuse since it occurs most strongly on 1NN sites, and c-STO is more spatially diffuse as it occurs most strongly on 2NN sites. The picture is similar in the tetragonal systems, wherein the greatest charge density change occurs on the 1NN Ti-site in t-PTO and the 1NN sites of t-BTO, though the charge density change in t-BTO appears to be nearly negligible. The structural effect is further investigated through analysis of the ionic displacement patterns.

D. Polaron-induced structural distortion

The A-site effects on the structure and displacement pattern of the polaron in each system are shown in Fig. 2. Therein, the ionic displacement relative to the bulk structure for each ion for the delocalized and polaron solutions are compared. The structural impact of the polaron may be assessed by looking at the difference between the polaron and delocalized figures for a given system. For example, in c-PTO [Figs. 2(c) and 2(h)], the displacement of the 1NN ions increases significantly between the delocalized and polaron solutions, indicating significant local atomic displacements from the localization of charge in the polaron picture. In c-STO [Figs. 2(a) and 2(f)] by contrast, the change in displacement of the 1NN ions between

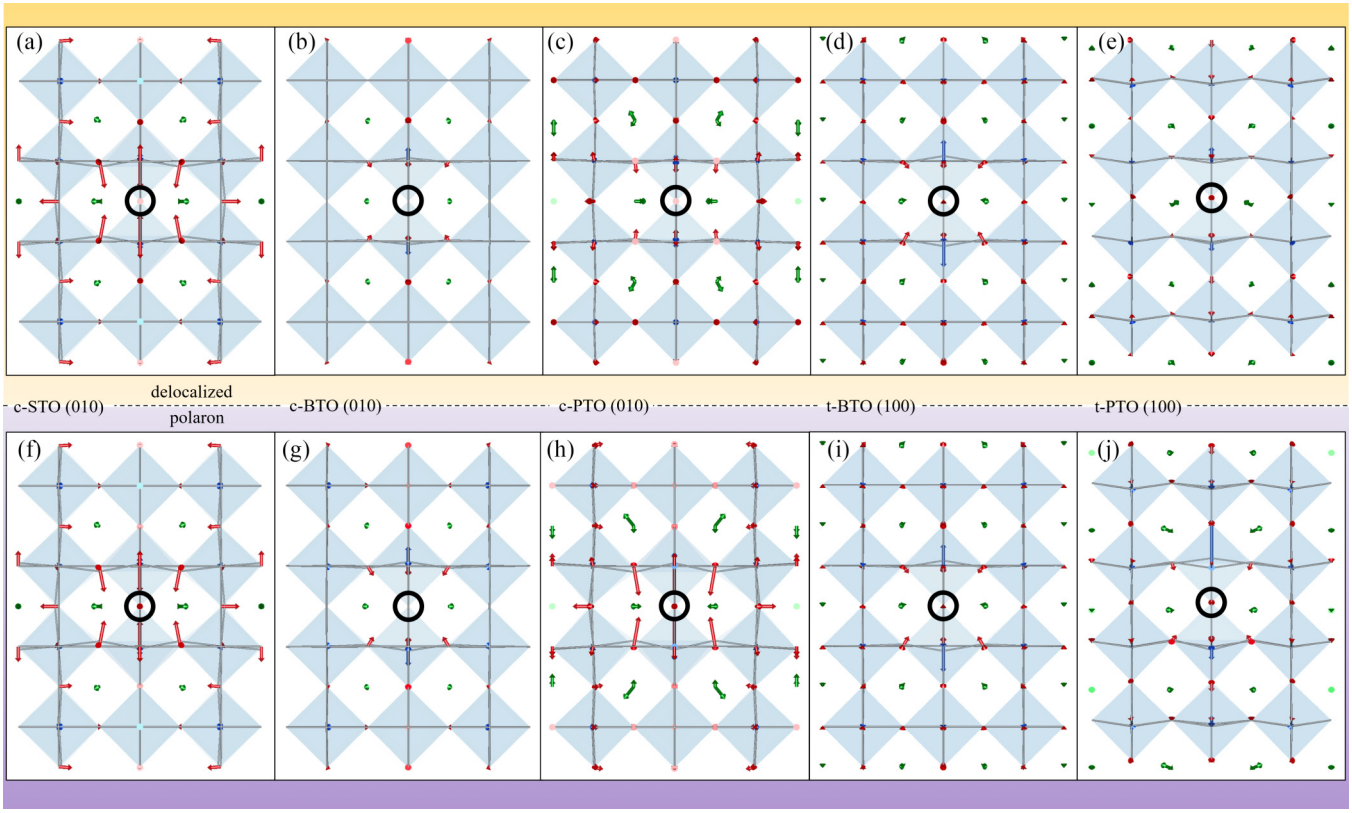

FIG. 2. The local atomic displacement relative to the bulk structure and structural details of each system are shown for the delocalized (top) and polaron (bottom) structures. The colored arrows, scaled by 5×, show the scaled magnitude and direction of displacement for selected atoms (green = A−site, blue = Ti, red = O, open circle = $V_{\ddot{O}}$). Note, there is a difference between the *c*/*a* ratios between the cubic and tetragonal systems, but each figure is scaled to be the same size for ease of comparison.

the polaron and delocalized pictures is very small. We observe that, in general, this ionic displacement due to the polaron, particularly that of the 1NNs, increases in magnitude with decreasing polaron formation energy.

The displacement of 1NN sites of the vacancy in the delocalized and polaron solutions are given in Table III with respect to the bulk, alongside the difference between them. In c-PTO, the displacements change by 0.19, 0.07, and 0.18 Å for the A-, Ti-, and O-sites, respectively, corresponding to a large magnitude of polaron formation energy, while the displacement difference in c-STO is < 0.01 Å for all sites (Table III, "Difference"), concomitant with a very small polaron formation energy magnitude. Meanwhile, the displacement of 1NN sites in c-BTO is between those of c-PTO and c-STO, coinciding with a mediate magnitude of polaron formation energy. Results for the tetragonal systems corroborate the same conclusion, with displacements of −0.02 Å or less for sites in t-BTO and significantly larger displacements of up to 0.34 Å in t-PTO. Therefore, we observe, again, the displacements of the 1NN ions in each system increase with decreasing polaron formation energy and are influenced directly by the species of the A-site. The delocalized structure displacements of c-STO relative to the bulk agree to within 0.01 Å of results obtained by Evarestov *et al.* [52] using hybrid functionals with a LCAO basis. The delocalized structure displacements in 1NN ions of c-PTO and t-PTO agree qualitatively with the results of Stashans *et al.* [56] using molecular orbital theory. Additionally, hybrid calculations performed by Choi *et al.* [57] using the plane-wave basis (as in this paper) agree that the

TABLE III. The displacements of the 1NN ions organized by site and system with respect to bulk. The difference between these is also given. The negative signs indicate motion toward the vacancy. All units are in Å.

	Delocalized			Polaron			Difference		
System	A-site (Δu)	Ti	O	A-site	Ti	O	A-site	Ti	O
c-STO	0.12	0.09	−0.27	0.11	0.10	−0.26	<−0.01	<0.01	<−0.01
c-BTO	0.05	0.15	−0.08	0.08	0.20	−0.12	0.03	0.05	−0.04
c-PTO	−0.15	0.07	−0.12	0.04	0.14	−0.30	0.19	0.07	−0.18
t-BTO	−0.07	0.27	−0.10	−0.07	0.28	−0.12	<−0.001	<0.01	−0.02
t-PTO	−0.11	0.18	−0.02	0.09	0.52	−0.08	0.2	0.34	−0.06

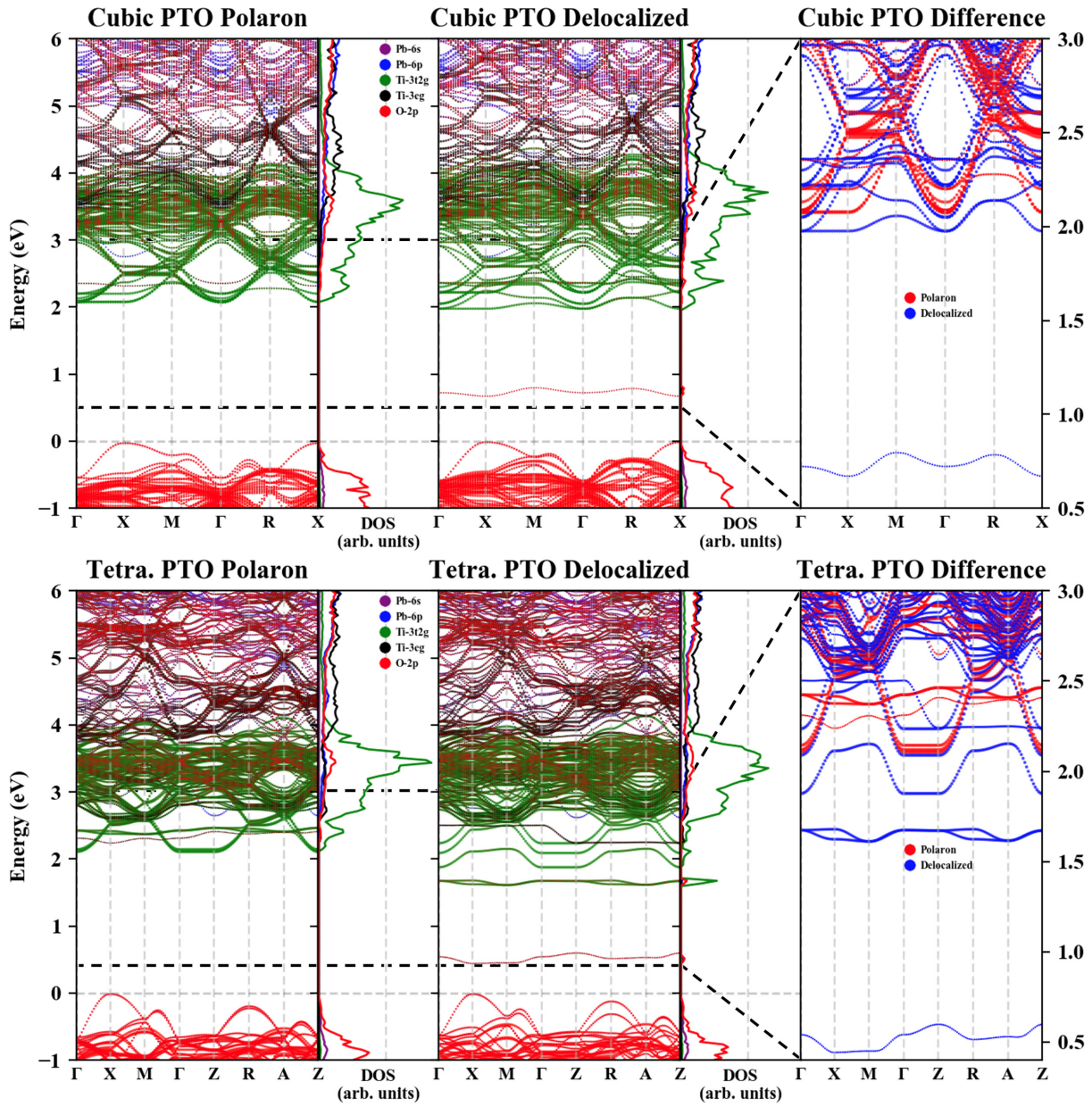

FIG. 3. The orbital-resolved density of states (DOS) and projected-band structures for the delocalized and polaron solutions of c-PTO and t-PTO. The Fermi energy is set to the valence band maximum (VBM), and a small window is plotted with both the polaron (red) and delocalized (blue) solutions to highlight the differences between them. Note states shown in the difference band structures are scaled to make the bands within the energy window most easily perceivable in the polaron or delocalized band structure.

structure of 1NN Ti-sites in c-BTO is symmetric about the vacancy.

E. Electronic structure influence from polaron

The orbital-resolved DOS and projected-band structure are calculated for each system to investigate the influence of the polaron on the electronic structure. In Figs. 3 and 4, these data for the polaron and delocalized structures are compared with one another, with the most important differences near the band gap highlighted in the "Difference" column of the figures. Consider c-PTO, the delocalized solution possesses an in-gap state at ~ 0.7 eV above the Fermi energy that relocates in the polaron solution to ~ 2.35 eV in the conduction bands (Fig. 3). Simultaneously, the conduction band minimum (CBM) increases in energy by ~ 0.1 eV in the polaron solution as more hybridization occurs in the states that comprise it. In t-PTO, the delocalized solution contains several in-gap states, at ~ 0.44, 1.66, and 1.88 eV, each of which move to positions within the conduction bands, ~ 2.23, 2.37, and 2.1 eV, with the highest energy in-gap state hybridizing with the CBM itself. These are the hallmarks of the influence of the polaron on the electronic structure of the delocalized picture: the relocation of a fictitious in-gap state or states to the conduction bands and an increase in energy of the CBM coupled with greater hybridization therein.

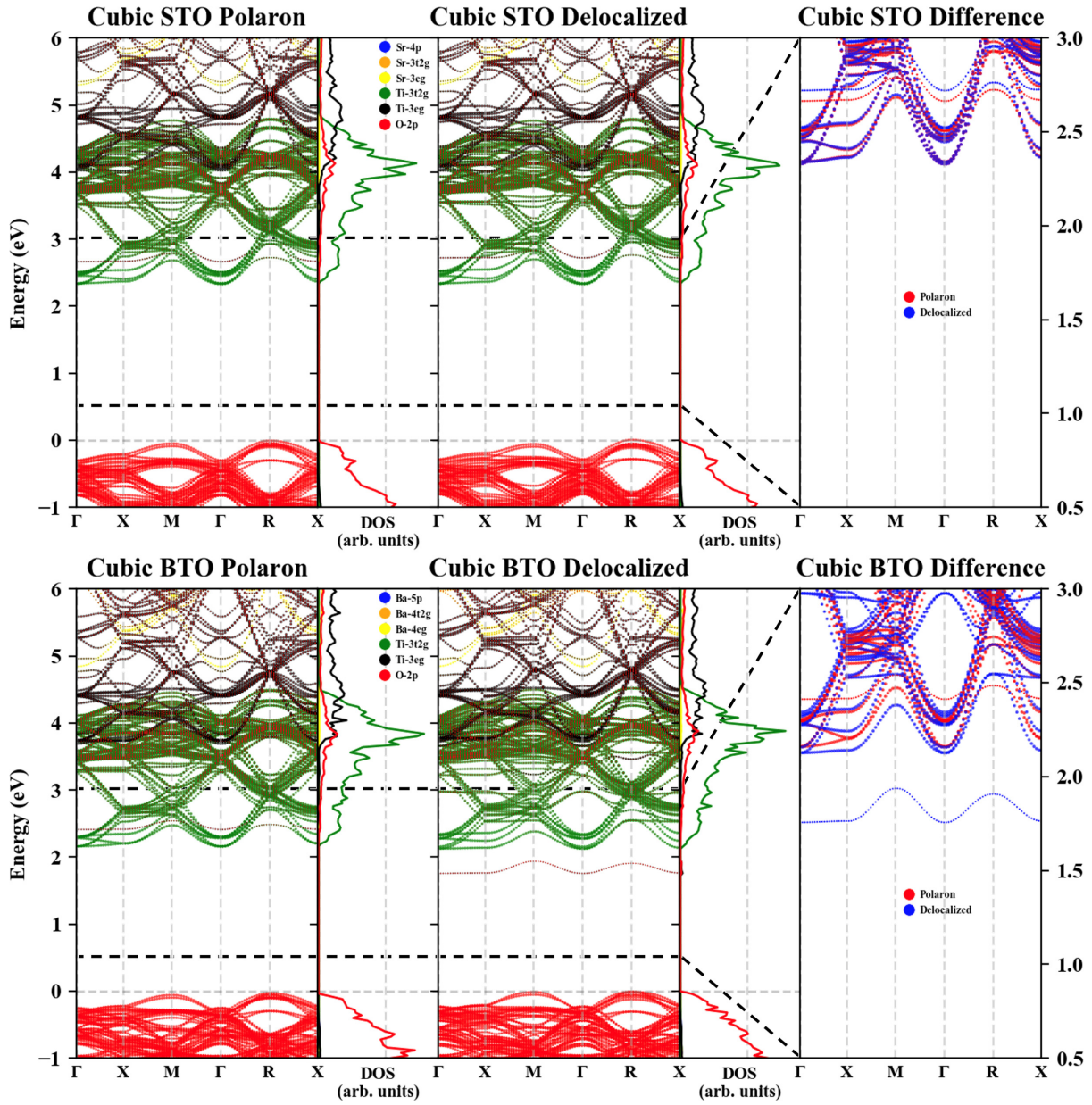

FIG. 4. The orbital-resolved density of states (DOS) and projected-band structures for the delocalized and polaron solutions of c-STO and c-BTO. The Fermi energy is set to the valence band maximum (VBM), and a small window is plotted with both the polaron (red) and delocalized (blue) solutions to highlight the differences between them. Note states shown in the difference band structures are scaled to make the bands within the energy window most easily perceivable in the polaron or delocalized band structure.

In c-BTO, the polaron solution possesses the same essential hallmarks as in the PTO systems, while the c-STO polaron solution has negligible effects on the band structure (Fig. 4). The in-gap state in c-BTO occurs at ~ 1.75 eV in the delocalized solution and relocates to ~ 2.42 eV in the polaron solution, in agreement with hybrid calculations from Choi *et al.* [57], suggesting the lack of a deep donor level in the band structure of c-BTO. However, c-STO possesses no in-gap state, the only minor difference being one state at ~ 2.72 eV in the delocalized solution lowering in energy to 2.67 eV in the polaron solution. The same is true of t-BTO, which is not shown because changes occurring in the conduction and valence bands near the band gap were found to be negligible. Therefore, we find that each system studied with a magnitude of polaron formation energy larger than a few millielectronvolts manifests a fictitious in-gap state or states in the delocalized solution.

The fictitious in-gap state characteristic of the delocalized solution is of primarily O$-2p$ character in the systems studied, though additional in-gap states of Ti-3d character exist in t-PTO. These in-gap states manifest in those systems with mediate or larger polaron energies: c-BTO, c-PTO, and t-PTO at 1.75, 0.7, and 0.5 eV. Comparatively, the polaron solution is generally characterized by the relocation of the in-gap state to within 1 eV of the CBM and an increase in energy and hybridization of the Ti-d_{xy}, d_{xz}, and d_{yz} (Ti-3d_{t2g})

bands forming the CBM. This occurs in each system containing an in-gap state in the delocalized solution, with the in-gap state relocating to 2.42 eV in c-BTO, 2.35 eV in c-PTO, and 2.23 eV in t-PTO. The additional in-gap states found in t-PTO at 1.66 and 1.88 eV also relocate to 2.37 and 2.1 eV, respectively, in the conduction bands of the polaron solutions. Based on these data, the in-gap state(s) present in the delocalized solution of each system is (are) found to be fictitious, that is, a byproduct of a nonphysical state caused by the delocalized descriptions employed in the standard DFT calculations. Therefore, a localized or semilocalized electron picture of a vacancy environment is required to obtain the correct physical picture.

Further analysis reveals electronic influence from A-site species contributes to the polaron energies, based on the number of states contributed in the projected DOS (pDOS) and occupation number in the projected bands near the gap from the A-site. This trend is shown most clearly in the cubic systems. In c-PTO, Pb-6*s* orbitals are found to contribute directly to the valence bands, while the Pb-6*p* bands contribute to the conduction bands, a result consistent with the GGA calculations of t-PTO by Wang *et al.* [58] and Hosseini *et al.* [59]. Pb-site orbital contributions correspond to the in-gap state in the delocalized solution at 0.7 eV and the relocated state in the polaron solution at 2.35 eV. The relocated state exhibits mixed O-2*p*, Ti-3d_{eg}, Pb-6*s*, and Pb-6*p* character, with the contribution from Ti-3d_{eg} increasing in the polaron solution. Comparatively, the A-site in c-BTO contributes no orbital character to any bands nearby the gap, though an in-gap state exists. A similar lack of electronic influence from the A-site near the gap is also observed in c-STO, concomitant with no in gap. Therefore, the direct orbital contribution of the A-site species near the band gap is taken to have a significant impact on the polaron formation energy, given the polaron formation energy difference between c-PTO (−1.688 eV) and c-BTO (−0.234 eV). This supports that the A-sites of both c-STO and c-BTO contribute primarily to the structure, and the differences between the delocalized and polaron pictures are due to the difference in ion size, whereas Pb appears to contribute both structurally and electronically.

A similar observation about the A-site can be made by observing the tetragonal systems. First, in t-BTO, there are no in-gap states in the delocalized structure, and only negligible change between the polaron and delocalized structures is observed (hence its absence from Fig. 3). This is significantly different from t-PTO, wherein three in-gap states exist, one of primarily Ti-3d_{t2g} character at 1.88 eV, a mixed state of both Ti-3d_{t2g} and O-2*p* character at 1.66 eV, and another at 0.44 eV of mixed Pb-6*s*, Pb-6*p*, Ti-3d_{eg}, and O-2*p* character. This further indicates the lack of electronic influence of Ba in polaron formation and the much stronger effect of the direct electronic interaction by Pb, agreeing neatly with the data obtained from the cubic systems.

IV. CONCLUSIONS

The polarons near vacancies in $ATiO_3$ perovskites are systematically studied to investigate the influence of the A-site ions on polaron stability, local atomic environment, and electronic properties. First, we have shown the polaron formation energy, as calculated via Eq. (3), changes by several orders of magnitude as the A-site is varied: t-PTO(−1.823)<c-PTO (−1.688 eV) < c-BTO(−0.234 eV) < c-STO(−0.007 eV) < t-BTO(−0.002 eV). The implication is twofold. First, the influence of polaron formation near vacancies in PTO systems is the strongest or possesses the greatest departure from the delocalized picture, while the mediate magnitude of the polaron formation energy in c-BTO implies weaker influence, and the small magnitude of the polaron formation energy in c-STO and t-BTO implies only very little change from the delocalized picture. Second, a critical role is played by the A-site influence on the polaron within these systems, which we investigate by comparing the charge density, ionic displacement, and projected bands of each system in the delocalized and polaron solutions.

These results imply the influence of the polaron on the charge density, local atomic displacement, and electronic structure in these systems can be tuned by the A-site. The response of the charge density increases in magnitude as the polaron formation energy decreases, and the ionic sites where the response is greatest changes with A-site species. Across the cubic systems, the charge density changes occur most in the 1NN A-sites in c-PTO (0.388 e/Å^3), 1NN Ti-sites in c-BTO (0.114 e/Å^3), and 2NN O-sites in c-STO (0.031 e/Å^3). As the polaron formation energy decreases, we observe an increase in the local ionic displacement around the vacancy, alongside a varying displacement pattern accompanying A-site species changes across both the cubic and tetragonal systems. For example, the largest displacement of 1NN ions in the cubic systems varies from 0.19 Å for the A-site in c-PTO, to 0.05 Å for Ti-site in c-BTO, and < 0.01 Å for all sites in c-STO. Analysis of projected band structures of the systems reveals the electronic structure influence from the polaron manifests itself through the relocation of a fictitious in-gap state or states found in the delocalized solution to the conduction bands in the polaron solution. These states are primarily O−2*p* character and decrease in energy with decreasing polaron formation energy from 2.35 eV above the VBM in c-PTO, to 2.42 eV in c-BTO, and 2.67 eV in c-STO. Furthermore, a larger magnitude of the polaron formation energy in the PTO systems is found to correspond to direct orbital contributions from A-site states in the system, showing that an increase in the number of states contributed by the A-site in the pDOS and projected bands correlates to an increase in the magnitude of the polaron formation energy.

In this paper, we demonstrate the localization of charge near charged vacancy sites producing additional local lattice and electronic structural changes reminiscent of polarons. We show the influence of the polarons on nearby vacancies in $ATiO_3$ perovskites may be subtly tuned using the A-site species to produce variations in the polaron stability, resulting in changes to the charge density, local atomic displacement, and electronic structure. This expanded understanding may be used to assist in effective functionalization of properties for which polarons are known to be important contributors in complex oxides (i.e., charge transport [10,12], photovoltaic interactions [4], and multiferroism [14]). However, additional work utilizing larger supercells to reduce any

supercell size effects, investigation of B-site species effects to expand the scope of the degrees of freedom studied, and direct calculations of electron-phonon coupling are required to investigate this picture of the oxygen vacancy more completely in these perovskite systems. Finally, utilizing the picture of trapped charge in the form of polarons at the interface of perovskite heterostructures, beginning with a systematic study of epitaxial strain effects on charge localization, could reveal mechanisms of interaction among the four principal degrees of freedom—lattice, charge, orbitals, and spin—with defects, leading to a more complete understanding of the roles played by defects at the interface.

ACKNOWLEDGMENTS

This paper is supported by the University of Tennessee Expanding Horizon program. This project used computational resources via the Infrastructure for Scientific Applications and Advanced Computing (ISAAC) Secure Enclave and ISAAC Next Gen at the University of Tennessee-Knoxville.

Dylan Windsor: methodology, software, validation, formal analysis, investigation, data curation, writing—original draft, visualization. Haixuan Xu: conceptualization, methodology, resources, writing—review and editing, supervision, project administration, funding acquisition.

[1] P. Zubko, S. Gariglio, M. Gabay, P. Ghosez, and J.-M. Triscone, Interface physics in complex oxide heterostructures, Annu. Rev. Condens. Matter Phys. **2**, 141 (2011).

[2] H. Y. Hwang, Y. Iwasa, M. Kawasaki, B. Keimer, N. Nagaosa, and Y. Tokura, Emergent phenomena at oxide interfaces, Nat. Mater. **11**, 103 (2012).

[3] R. Ramesh and D. G. Schlom, Creating emergent phenomena in oxide superlattices, Nat. Rev. Mater. **4**, 257 (2019).

[4] E. Pastor, M. Sachs, S. Selim, J. R. Durrant, A. A. Bakulin, and A. Walsh, Electronic defects in metal oxide photocatalysts, Nat. Rev. Mater. **7**, 503 (2022).

[5] T. Xu, T. Shimada, Y. Araki, J. Wang, and T. Kitamura, Multiferroic domain walls in ferroelectric $PbTiO_3$ with oxygen deficiency, Nano Lett. **16**, 454 (2016).

[6] T. Shimada, Y. Uratani, and T. Kitamura, Vacancy-driven ferromagnetism in ferroelectric $PbTiO_3$, Appl. Phys. Lett. **100**, 162901 (2012).

[7] L. Zhang, I. Bredeson, A. Y. Birenbaum, P. R. C. Kent, V. R. Cooper, P. Ganesh, and H. Xu, Oxygen vacancy formation energies in $PbTiO_3/SrTiO_3$ superlattice, Phys. Rev. Mater. **2**, 064409 (2018).

[8] J. R. De Lile, A. Bahadoran, S. Zhou, and J. Zhang, Polaron in TiO_2 from first-principles: A review, Adv. Theory Simul. **5**, 2100244 (2022).

[9] C. Franchini, M. Reticcioli, M. Setvin, and U. Diebold, Polarons in materials, Nat. Rev. Mater. **6**, 560 (2021).

[10] Y. Natanzon, A. Azulay, and Y. Amouyal, Evaluation of polaron transport in solids from first-principles, Isr. J. Chem. **60**, 768 (2020).

[11] W. H. Sio, C. Verdi, S. Ponce, and F. Giustino, Polarons from First Principles, without Supercells, Phys. Rev. Lett. **122**, 246403 (2019).

[12] V. Coropceanu, J. Cornil, D. A. Da Silva Filho, Y. Olivier, R. Silbey, and J.-L. Bredas, Charge transport in organic semiconductors, Chem. Rev. **107**, 926 (2007).

[13] J. M. D. Teresa, M. R. Ibarra, P. A. Algarabel, C. Ritter, C. Marquina, J. Blasco, J. Garcia, A. Del Moral, and Z. Arnold, Evidence for magnetic polarons in the magnetoresistive perovskites, Nature (London). **386**, 256 (1997).

[14] K. Miyata and X.-Y. Zhu, Ferroelectric large polarons, Nat. Mater. **17**, 379 (2018).

[15] M. Reticcioli, I. Sokolović, M. Schmid, U. Diebold, M. Setvin, and C. Franchini, Interplay between Adsorbates and Polarons: CO on Rutile TiO_2(110), Phys. Rev. Lett. **122**, 016805 (2019).

[16] M. Setvin, C. Franchini, X. Hao, M. Schmid, A. Janotti, M. Kaltak, C. G. Van De Valle, G. Kresse, and U. Diebold, Direct View at Excess Electrons in TiO_2 Rutile and Anatase, Phys. Rev. Lett. **113**, 086402 (2014).

[17] S. Moser, L. Moreschini, J. Jacimovic, O. S. Barisic, H. Berger, A. Magrez, Y. J. Chang, K. S. Kim, A. Bostwick, E. Rotenberg *et al.*, Tunable Polaronic Conduction in Anatase TiO_2, Phys. Rev. Lett. **110**, 196403 (2013).

[18] A. Janotti, J. B. Varley, P. Rinke, N. Umezawa, G. Kresse, and C. G. Van de Walle, Hybrid functional studies of the oxygen vacancy in TiO_2, Phys. Rev. B **81**, 085212 (2010).

[19] L. L. Rusevich, M. Tyunina, E. A. Kotomin, N. Nepomniashchaia, and A. Dejneka, The electronic properties of $SrTiO_{3-\delta}$ with oxygen vacancies or substitutions, Sci. Rep. **11**, 23341 (2021).

[20] H. E. Weaver, Dielectric properties of single crystals of $SrTiO_3$ at low temperatures, J. Phys. Chem. Solids **11**, 274 (1959).

[21] D. Zhang, Z.-K. Han, G. E. Murgida, M. V. Ganduglia-Pirovano, and Y. Gao, Oxygen-Vacancy Dynamics and Entanglement with Polaron Hopping at the Reduced CeO_2(111) Surface, Phys. Rev. Lett. **122**, 096101 (2019).

[22] D. K. Zhong, S. Choi, and D. R. Gamelin, Near-complete suppression of surface recombination in solar photoelectrolysis by "Co-Pi" catalyst-modified W:$BiVO_4$, J. Am. Chem. Soc. **133**, 18370 (2011).

[23] H. L. Tuller and A. S. Nowick, Small polaron electron transport in reduced CeO_2 single crystals, J. Phys. Chem. Solids **38**, 859 (1977).

[24] P. Nagels, M. Denayer, and J. Devreese, Electrical properties of single crystals of uranium dioxide, Solid State Commun. **1**, 35 (1963).

[25] H. P. R. Frederikse, W. R. Thurber, and W. R. Hosler, Electronic transport in strontium titanate, Phys. Rev. **134**, A442 (1964).

[26] M. Reticcioli, M. Setvin, X. Hao, P. Flauger, G. Kresse, M. Schmid, U. Diebold, and C. Franchini, Polaron-Driven Surface Reconstructions, Phys. Rev. X **7**, 031053 (2017).

[27] V. N. Strocov, C. Cancellieri, and A. S. Mishchenko, Electrons and polarons at oxide interfaces explored by soft-x-ray ARPES, in *Spectroscopy of Complex Oxide Interfaces*, edited by C. Cancellieri and V. Strocov (Springer, Cham, 2018), pp. 107–151.

[28] S. L. Dudarev, G. A. Botton, S. Y. Savrasov, C. J. Humphreys, and A. P. Sutton, Electron-energy-loss spectra and the structural

stability of nickel oxide: An LSDA+U study, Phys. Rev. B **57**, 1505 (1998).
[29] A. Filippetti and N. A. Spaldin, Self-interaction-corrected pseudopotential scheme for magnetic and strongly-correlated systems, Phys. Rev. B **67**, 125109 (2003).
[30] J. P. Perdew and A. Zunger, Self-interaction correction to density-functional approximations for many-electron systems, Phys. Rev. B **23**, 5048 (1981).
[31] D. I. Bilc, R. Orlando, R. Shaltaf, G.-M. Rignanese, J. Iniguez, and P. Ghosez, Hybrid exchange-correlation functional for accurate prediction of the electronic and structural properties of ferroelectric oxides, Phys. Rev. B **77**, 165107 (2008).
[32] N. A. Deskins and M. Dupuis, Electron transport via polaron hopping in bulk TiO_2: A density functional theory characterization, Phys. Rev. B **75**, 195212 (2007).
[33] T. Xu, T. Shimada, Y. Araki, M. Mori, G. Fujimoto, J. Wang, T.-Y. Zhang, and T. Kitamura, Electron engineering of metallic multiferroic polarons in epitaxial $BaTiO_3$, npj Comput. Mater. **5**, 23 (2019).
[34] P. E. Blöchl, Projector augmented-wave method, Phys. Rev. B **50**, 17953 (1994).
[35] G. Kresse and J. Furthmüller, Efficiency of *ab-initio* total energy calculations for metals and semiconductors using a plane-wave basis set, Comput. Mater. Sci. **6**, 15 (1996).
[36] G. Kresse and J. Furthmüller, Efficient iterative schemes for *ab initio* total-energy calculations using a plane-wave basis set, Phys. Rev. B **54**, 11169 (1996).
[37] J. P. Perdew, K. Burke, and M. Ernzerhof, Generalized Gradient Approximation Made Simple, Phys. Rev. Lett. **77**, 3865 (1996).
[38] J. P. Perdew, A. Ruzsinszky, G. I. Csonka, O. A. Vydrov, G. E. Scuseria, L. A. Constantin, X. Zhou, and K. Burke, Restoring the Density-Gradient Expansion for Exchange in Solids and Surfaces, Phys. Rev. Lett. **100**, 136406 (2008).
[39] L. Zhang, B. Liu, H. Zhuang, P. R. C. Kent, V. R. Cooper, P. Ganesh, and H. Xu, Oxygen vacancy diffusion in bulk $SrTiO_3$ from density functional theory calculations, Comput. Mater. Sci. **118**, 309 (2016).
[40] X. Hao, Z. Wang, M. Schmid, U. Diebold, and C. Franchini, Coexistence of trapped and free excess electrons in $SrTiO_3$, Phys. Rev. B **91**, 085204 (2015).
[41] J. P. Buban, H. Iddir, and S. Öğüt, Structural and electronic properties of oxygen vacancies in cubic and antiferrodistortive phases of $SrTiO_3$, Phys. Rev. B **69**, 180102(R) (2004).
[42] K. Momma and F. Izumi, VESTA 3 for three-dimensional visualization of crystal, volumetric and morphology data, J. Appl. Cryst. **44**, 1272 (2011).
[43] C. M. Culbertson, A. T. Flak, M. Yatskin, P. H.-Y. Cheong, D. P. Cann, and M. R. Dolgos, Neutron total scattering studies of group II titanates ($ATiO_3$, $A^2+ =$ Mg, Ca, Sr, Ba), Sci. Rep. **10**, 3729 (2020).
[44] Q.-J. Liu, N.-C. Zhang, F.-S. Liu, H.-Y. Wang, and Z.-T. Liu, $BaTiO_3$: Energy, geometrical and electronic structure, relationship between optical constant and density from first-principles calculations, Opt. Mater. **35**, 2629 (2013).
[45] A. Aimi, K. Horiuchi, Y. Yamaguchi, S. Ito, and K. Fujimoto, Disordered off-center direction of Ti^{4+} in pseudo-cubic type $BaTiO_3$ prepared by mixed hydroxide process, J. Ceram. Soc. Jpn. **129**, 73 (2021).
[46] J. J. Brown, Z. Ke, W. Geng, and A. J. Page, Oxygen vacancy defect migration in titanate perovskite surfaces: Effect of the A-site cations, J. Phys. Chem. C **122**, 14590 (2018).
[47] S. Piskunov, E. Heifets, R. I. Eglitis, and G. Borstel, Bulk properties and electronic structure of $SrTiO_3$, $BaTiO_3$, $PbTiO_3$ perovskites: An *ab initio* HF/DFT study, Comput. Mater. Sci. **29**, 165 (2004).
[48] Y. Kuroiwa, S. Aoyagi, A. Sawada, J. Harada, E. Nishibori, M. Takata, and M. Sakata, Evidence for Pb-O Covalency in Tetragonal $PbTiO_3$, Phys. Rev. Lett. **87**, 217601 (2001).
[49] Q.-L. Fang, J.-M. Zhang, and K.-W. Xu, Vacancy and doping driven ferromagnetism in $BaTiO_3$ perovskite, Physica B **424**, 79 (2013).
[50] Z. Alahmed and H. Fu, First-principles determination of chemical potentials and vacancy formation energies in $PbTiO_3$ and $BaTiO_3$, Phys. Rev. B **76**, 224101 (2007).
[51] S. Tomoda, T. Shimada, T. Ueda, J. Wang, and T. Kitamura, Hybrid functional study on the ferroelectricity of domain walls with O-vacancies in $PbTiO_3$, Mech. Eng. J. **2**, 15 (2015).
[52] R. Evarestov, E. Blokhin, D. Gryaznov, E. A. Kotomin, J. Merkle, and R. Maier, Jahn-Teller effect in the phonon properties of defective $SrTiO_3$ from first principles, Phys. Rev. B **85**, 174303 (2012).
[53] D. M. Smyth, Defect structure in perovskite titanates, Curr. Opin. Solid State Mater. Sci. **1**, 692 (1996).
[54] H. I. Yoo, Hole-trapping effect on thermoelectric power of mixed ionic electronic conductor $BaTiO_3$, Phys. Chem. Chem. Phys. **7**, 3888 (2005).
[55] H. I. Yoo and C.-R. Song, Thermoelectricty of $BaTiO_{3+\delta}$, J. Electroceram. **6**, 61 (2001).
[56] A. Stashans, S. Serrano, and P. Medina, A quantum-chemical study of oxygen-vacancy defects in $PbTiO_3$ crystals, Physica B **381**, 82 (2006).
[57] M. Choi, F. Oba, and I. Tanaka, Electronic and structural properties of the oxygen vacancy in $BaTiO_3$, Appl. Phys. Lett. **98**, 172901 (2011).
[58] L. Wang, P. Yuan, F. Wang, E. Liang, Q. Sun, Z. Guo, and Y. Jia, First-principles study of tetragonal $PbTiO_3$: Phonon and thermal expansion, Mater. Res. Bull. **49**, 509 (2014).
[59] S. M. Hosseini, T. Movlarooy, and A. Kompany, First-principle calculations of the cohesive energy and the electronic properties of $PbTiO_3$, Physica B **391**, 316 (2007).